Phytoplankton communities and acclimation in a cyclonic eddy in the southwest Indian Ocean

R. Barlow[a,b,*], T. Lamont[c,b], M-J. Gibberd[b], R. Airs[d], L. Jacobs[c], K. Britz[c]

[a]Bayworld Centre for Research & Education, 5 Riesling Road, Constantia 7806, Cape Town, South Africa
[b]Marine Research Institute & Department of Oceanography, University of Cape Town, Private Bag X3, Rondebosch 7701, South Africa
[c]Oceans and Coastal Research, Department of Environmental Affairs, Private Bag X4390, Cape Town, 8000, South Africa
[d]Plymouth Marine Laboratory, Prospect Place, West Hoe, Plymouth PL1 3DH, United Kingdom
*E-mail: rgb.barlow@gmail.com

ABSTRACT

A study of phytoplankton in a cyclonic eddy was undertaken in the Mozambique Basin between Madagascar and southern Africa during austral winter. CHEMTAX analysis of pigment data indicated that the community comprised mainly haptophytes and diatoms, with *Prochlorococcus*, prasinophytes and pelagophytes also being prominent to the east and west of the eddy. There was little difference in community structure, chlorophyll-specific absorption [$a^*_{ph}(440)$] and pigment:TChla ratios between the surface and the sub-surface chlorophyll maximum (SCM), reflecting acclimation to fluctuating light conditions in a well mixed upper layer. Values for $a^*_{ph}(440)$ were low for diatom dominance, high where prokaryote proportion was high, and intermediate for flagellate dominated communities. Chlorophyll *c* and fucoxanthin:TChla ratios were elevated over most of the eddy, while 19'-hexanoyloxyfucoxanthin ratios increased in the eastern and western sectors. In a community comprising mainly flagellates and *Prochlorococcus* to the west of the eddy, there was high $a^*_{ph}(440)$ at the surface and elevated ratios for divinyl chlorophyll *a*, chlorophyll *b* and 19'-hexanoyloxyfucoxanthin at the SCM. An increase in diadinoxanthin:TChla ratios and a decline in the quantum efficiency of photochemistry in PSII under high light conditions, indicated some photoprotection and photoinhibition at the surface even in a well mixed environment. Diadinoxanthin was the main photoprotective carotenoid within the eddy, while zeaxanthin was the dominant photoprotective pigment outside the eddy. The results of this study will be useful inputs into appropriate remote sensing models for estimating primary production and the size class distribution of phytoplankton in eddies in the southwest Indian Ocean.

Keywords: Phytoplankton, Pigments, Absorption, Active fluorescence, Cyclonic eddy, Indian Ocean

1. Introduction

Early research in the southwest Indian Ocean indicated that there is a southern extension of the South East Madagascar Current (SEMC) across the northern part of the Mozambique Basin (MB) (Duncan, 1970; Wyrtki, 1971). Deep sea eddies also occur in the MB (Grundlingh, 1985) and both cyclonic and anticyclonic eddies can originate in the Mozambique Channel (Schouten et al. 2002) and move in a southerly or westerly direction (Grundlingh et al. 1991). De Ruijter et al., (2005) also noted an abundance of eddies to the south and southwest of Madagascar, with the cyclones and anticyclones propagating towards southern Africa. These eddies can appear as dipole pairs (De Ruijter et al., 2004; Ridderinkhof et al., 2013) and the cyclonic eddies are usually formed as lee eddies on the inshore edge of the SEMC (De Ruijter et al., 2004).

To the north, more recent investigations in the Mozambique Channel showed that anticyclonic eddies are very prominent and cyclonic eddies are usually present in a dipole pair (Ternon et al., 2014). Independent cyclonic eddies can occur and it appears that southward drifting anticyclonic eddies occur mainly on the western side of the Channel, while the distribution of cyclonic eddies is more ubiquitous, with a slight tendency toward greater occurrence to the east closer to Madagascar (Halo et al., 2014; Hanke et al.,

2014). Phytoplankton studies revealed that chlorophyll *a* concentrations were low in surface waters, with sub-surface levels being significantly greater (Lamont et al., 2014). Pigment indices indicated that prokaryotes were the most significant phytoplankton group at the surface, with small flagellates being of secondary importance, while flagellates dominated at the DCM, except for some diatom domination close to the coast (Barlow et al., 2014). These prokaryote dominated communities displayed a large range in the proportion of chlorophyll *a* within the total pigment pool and a high proportion of photoprotective carotenoids, while diatoms had relatively high proportions of chlorophyll *a*, photosynthetic carotenoids and chlorophyll c. Flagellate dominated communities had a lower proportion of chlorophyll *a*, increased levels of photosynthetic carotenoids and intermediate proportion of chlorophyll *c* (Barlow et al., 2014). Similar adaptations have been observed in a shelf sea where picoeukaryote-*Synechococcus* communities in the surface mixed layer had more photoprotective carotenoids, while flagellates and diatoms >5 µm at the deep chlorophyll maximum contained a high proportion of photosynthetic carotenoids (Hickman et al., 2009).

Variability in the photosynthetic performance of phytoplankton depends on changes in both the taxonomic composition of communities and prevailing environmental conditions. The functional absorption cross-section of photosystem II (σ_{PSII}) can vary as a result of spatial taxonomic differences, whereas electron transport rates usually decrease with depth from the surface to the subsurface chlorophyll maximum in stratified waters (Moore et al., 2006). In contrast, communities within a mixed water column that is characterised by low mean irradiance actually acclimate to relatively high irradiance (Moore et al., 2006). Electron transport rates are closely linked to the diurnal cycle of light availability, however, with peak rates occurring at about solar noon in surface communities (Schuback et al., 2016). In populations where microphytoplankton usually dominate, it was noted that σ_{PSII} and the maximum photochemical efficiency generally increased with depth, while electron transport rates were greater near the surface under elevated irradiance but decreased progressively as irradiance decreased deeper in the water column (Zhu et al., 2016), complementing the observations of Moore et al. (2006).

No detailed studies of phytoplankton have been undertaken in eddies in the MB, and particularly not in cyclonic eddies that are generated near Madagascar. An opportunity arose to undertake an investigation in such an eddy during an austral winter research cruise between South Africa and Madagascar (Fig. 1). The objective of the study was to use pigment, absorption and active fluorescence data to understand some aspects of the acclimation of phytoplankton communities to environmental conditions in the eddy. The following scientific questions were posed: (1) What is the community structure within and outside the eddy? (2) Are there significant differences in the absorption and pigment characteristics between the surface and the sub-surface chlorophyll maximum? (3) How variable is photosynthetic activity across the eddy?

2. Methods

2.1. Hydrography and sampling

Hydrographic measurements were conducted at 25 stations spaced at 18.52 km intervals on a transect through the eddy during 17-23 July 2013 (Figs. 1 & 2) with water column profiling of temperature, salinity, photosynthetically available radiation (PAR) and fluorescence during CTD deployments. Fluorescence data was converted to chlorophyll equivalents by scaling to the chlorophyll *a* concentrations measured by HPLC. Conservative temperature (°C) and absolute salinity (S_A (g kg^{-1})) were calculated from in situ temperature and salinity profiles, according to the new thermodynamic equation of seawater (IOC et al., 2010). Nutrient samples were taken at selected depths and stored frozen at -80^{o}C for later analysis ashore using standard auto-analyser techniques (Mostert, 1983). Seawater samples were collected at the surface and at a sub-surface chlorophyll maximum (SCM) only for pigment, absorption and active fluorescence analysis. CTD fluorescence profiles did not display a distinct deep chlorophyll maximum at most of the stations but only a broad vertical band of sub-surface chlorophyll. A depth at approximately the middle of this broad band was therefore selected for samples to represent phytoplankton deeper in the

water column. Active fluorescence measurements were conducted on board, while pigment and absorption samples were stored frozen at -80^{o}C for analysis ashore.

The depth of the upper mixed layer (Z_m) was determined as the depth where the local change in density was ≥0.03 kg m^{-3} using potential density profiles and a threshold gradient criterion (Thomson and Fine, 2003). CTD profiling was undertaken both during the day and night and so for consistency the depth of the euphotic zone (Z_e), defined where irradiance is 1% of the surface value, was estimated from the vertical chlorophyll *a* profiles, according to Morel and Berthon (1989). This relationship was approximated by two successive linear segments, using the modified coefficients of Morel and Maritorena (2001), and Z_e was derived for each vertical profile.

2.2. Pigment analysis and CHEMTAX

Pigments were extracted in 90 % acetone, aided by the use of ultrasonication, clarified by centrifugation and filtration, and analysed by HPLC (ThermoScientific Accela) using a Waters Symmetry C8 column (150 x 2.1 mm, 3.5 µm particle size, thermostated at 25^{o}C) according to Zapata et al. (2000). Pigments were detected at 440 and 660 nm and identified by retention time and on-line diode array spectra. Monovinyl chlorophyll *a* standard was obtained from Sigma-Aldrich Ltd and other pigment standards were purchased from the DHI Institute for Water and Environment, Denmark. Quality assurance protocols followed Van Heukelem and Hooker (2011). The method separates divinyl and monovinyl chlorophyll a, zeaxanthin and lutein, but does not resolve divinyl and monovinyl chlorophyll *b*. Therefore the chlorophyll *b* data is monovinyl plus divinyl chlorophyll *b*. Limits of detection were of the order of 0.001 mg m^{-3}.

To determine community composition, pigment data was analysed by CHEMTAX (Mackey et al., 1996) following Higgins et al. (2011), with chemotaxonomic groups being identified according to Jeffrey et al. (2011). An assumption made using CHEMTAX is that the pigment:chlorophyll *a* ratios are constant across all the samples within each analysis. Samples were therefore separated by depth such that all surface and all SCM samples were each run together. Pigment starting ratios were obtained from Higgins et al. (2011) and Table 1 indicates the identified functional groups and the various starting and output ratios for each group. Although *Prochlorococcus* is also a cyanobacterium, the distinct divinyl chlorophyll *a* signature allows *Prochlorococcus* to be distinguished from *Synechococcus* in the CHEMTAX analysis. To ease the presentation of the chemotaxonomic data, diatoms-1 and -2 were combined into a collective diatom group, and prasinophytes-1 and -3 were combined into a collective prasinophyte group. Data for chlorophytes is not presented as CHEMTAX indicated that the contribution of this group was very low.

CHEMTAX outputs are the fraction of chlorophyll *a* attributed to each functional group specified in the matrix. The HPLC method separated monovinyl chlorophyll *a* allomer, monovinyl chlorophyll *a*, monovinyl chlorophyll *a* epimer and chlorophyllide *a*, and in CHEMTAX the sum of all 4 was used as the chlorophyll *a* concentration. Divinyl chlorophyll *a* was allocated entirely to *Prochlorococcus* spp. TChla was used as an index of phytoplankton biomass and is the sum of chlorophyll *a* plus divinyl chlorophyll *a*. The software may not discover the best global solution if it encounters local minima in the process. To circumvent this possibility, multiple starting points were used. Sixty-nine further pigment ratio tables were generated by multiplying each cell of the initial table by a randomly determined factor F, calculated as:

$$F = 1 + S \times (R - 0.5)$$

where S is a scaling factor of 0.7, and R is a random number between 0 and 1 generated using the Microsoft Excel RAND function (Wright et al., 2009). Each of the 60 ratio tables was used as the starting point for a CHEMTAX optimization. The solution with the smallest residual was used for the estimated taxonomic abundance.

2.3. Absorption and active fluorescence

Particulate absorption [$a_p(\lambda)$] spectra (400-750 nm) were determined by the quantitative filter technique (QFT) of Tassan and Ferrari (1995) using a spectrophotometer (GBC Cintra 404) equipped with an integrating sphere. Pigments were removed by bleaching with sodium hypochlorite and rescanned to measure the detrital absorption. All spectra were corrected by subtracting blank GF/F spectra and 750 nm values from all wavelengths according to Roesler (1998). The path length amplification factor (β) recommended by Roesler (1998) was used to correct for scattering by the glass fibre filters. Phytoplankton absorption coefficients [$a_{ph}(\lambda)$] were estimated by subtracting detrital absorption [$a_d(\lambda)$] from the $a_p(\lambda)$ spectra. Chlorophyll-specific absorption [$a^*_{ph}(\lambda)$] was calculated by normalising $a_{ph}(\lambda)$ to TChla.

A number of empirically derived β factors have been reported in the literature (Bricaud and Stramski, 1990; Cleveland and Weidemann, 1993; Mitchell and Kiefer, 1988; Moore et al., 1995) but these published results are inconsistent and β is probably the largest source of error in estimating absorption coefficients. Empirical derivations are based on the relationship between the optical density of cells in suspension in a cuvette and those collected on glass-fibre filters, but corrections need to be derived for scattering losses and path-length amplification in the cuvette and these are not straightforward to determine and can lead to significant errors. In contrast, particles on a filter do little to change the optical path length of the filter pad as scattering by the pad dominates the path-length amplification (Roesler, 1998). Therefore, a single β factor for filter pads can be determined that would apply to all samples, independent of specific particles. Roesler (1998) used a theoretical approach to estimate path-length amplification from the average cosine of diffusely travelling photons in the filter pad and deduced a value of 2. This new value was tested by estimating $a_{ph}(\lambda)$ for a range of cultures and field samples (1–20 μm size) using the modified QFT and comparing $a_{ph}(\lambda)$ determined with an ac-9 meter of 25 cm pathlength (WETLabs). Linear regressions were highly significant (r^2 >0.99) and the estimated slope and intercept were not significantly different from 1 and 0 respectively (P <0.001) (Roesler, 1998). This author stated that the use of the QFT with the new value for β yields accurate estimates of $a_{ph}(\lambda)$ irrespective of the concentration and composition of the particulate material. Using an empirical approach, Bricaud and Stramski (1990) also reported that a β factor of around 2 was suitable for correction of path length amplification for various population sizes.

Reconstructed absorption spectra for 13 individual pigments [$a_{pig}(\lambda)$] were estimated according to

$$a_{pig}(\lambda) = a_i^*(\lambda)\, C_i \,,$$

where $a_i^*(\lambda)$ ($m^2\ mg^{-1}$) is the *in vivo*, weight-specific, absorption coefficient of the individual pigments as reported by Bricaud et al. (2004) and C_i ($mg\ m^{-3}$) are the pigment concentrations. Specific absorption [$a^*_{pig}(\lambda)$] was calculated by normalising $a_{pig}(\lambda)$ to TChla.

Active fluorescence measurements were made with a bench-top FIRe fluorometer (Gorbunov and Falkowski, 2004) on discrete samples that were dark-adapted for >30 min prior to measurement. The FIRe protocol involves a strong flash of saturating blue light (452 +/- 30 nm) that causes a rise in fluorescence *in vivo* from an initial (Fo) to a maximum (Fm) level on the time-scale of a single photosynthetic turnover, <100 μs. This change in fluorescence (Fv = Fm-Fo) is associated with absorption and utilization of light energy in photosynthesis and is normalized to Fm (Fv/Fm) to deduce the maximum quantum efficiency of photochemistry in PSII (Kolber et al., 1998). Functional absorption cross-sections of PSII ($\sigma_{PSII,452}$ $10^{-20}\ m^2\ quanta^{-1}$) are derived from the rate at which fluorescence increases from Fo to Fm. Following the termination of the saturating flash, the fluorescence yield relaxation is recorded, which reflects the time constant of electron transport on the acceptor side of PSII (τ_{Qa}), i.e. the reoxidation of the primary PSII electron acceptor Q_a (Kolber et al., 1998). Blanks were prepared by filtering seawater through GF/F filters and treated exactly as the other samples for dark adaptation and gain settings. Excitation profiles were established for all gain settings using chlorophyll *a* standards. Raw data, including blanks, were processed with the FIRe software such that the averaged signals from 25

unique iterations from the same sample were produced to yield Fv/Fm, σ_{PSII} and τ_{Qa}. The rate of Q_a reoxidation was estimated as $1/\tau_{Qa}$ (ms^{-1}).

3. Results

3.1. Hydrography

At the time of the study, the eddy was located in the vicinity of 27°S, 40.5°E close to the SEMC that flows in a southwesterly direction beyond the shelf edge to the south of Madagascar (Fig. 1a). Interaction between the cyclonic eddy and the SEMC (Fig. 1a) resulted in water with elevated chlorophyll being advected from the Madagascar shelf along the inshore edge of the Current, and entrained into the eddy (Fig. 1b). The eddy was observed to drift in a southwesterly direction and therefore the position of the sampling stations had to be slightly adjusted accordingly during the study period. Fig. 2a,b shows a close up of station positions in relation to the sea-surface height and cyclonic flow in the eddy for 17 and 22 July 2013 respectively, while Fig. 2c,d shows the weekly averaged satellite chlorophyll *a* for 12-19 July and 20-27 July 2013.

The conservative temperature across the eddy to 1000 m is presented in Fig. 3 and the upward doming of the isotherms that is typical of cyclonic eddies may be noted. The 9°C isotherm is highlighted to illustrate this doming. The doming did not penetrate to the surface but only reached to about 100 m, coinciding approximately with the depth of Z_m, as shown in the more detailed temperature pattern in Fig. 4a and more clearly indicated by the uplift of elevated nitrates below 100m (Fig. 4b). The uniform temperature within the upper 75-100 m is indicative of a well mixed water column and confirmed by the depth of Z_m being deeper than the depth of Z_e (Fig. 4a). This mixing was induced by strong southeasterly winds that prevailed in July 2013.

Satellite data indicated that the eddy boundaries over the study period were located at 41.9°E in the east on 17 July 2013 (Fig. 2a) and at 38.9°E in the west on 22 July 2013 (Fig. 2b). This means that 4 stations were sampled outside the eddy to the east (Fig. 2a, c) and 2 stations were sampled outside the eddy to the west (Fig. 2b,d). Nutrient concentrations were generally low within the Z_m, particularly for nitrates that were <0.1 mmol m^{-3} in the upper 75-100 m (Fig. 4b). Nitrite levels were variable, however, but higher than nitrate at various locations, reaching 0.25 mmol m^{-3} at 25 m in the vicinity of 39.5°E (Fig. 4c). The nutriclines below 75 m in Fig. 4b,c display a clear doming that demarcates the location of the eddy between 38.9°E and 41.9°E.

The elevated but patchy chlorophyll *a* pattern as determined from the converted fluorescence profiles indicated the distribution of the phytoplankton within the eddy, with the highest levels in the core at ~40°E (Fig 4d). No distinct deep chlorophyll maximum was observed, however, and chlorophyll *a* was lower on the eastern side of the eddy with patchy distribution. A deep chlorophyll maximum was observed to the west of the eddy at 38.73°E, with significantly low chlorophyll *a* in the upper water column at this locality (Fig. 4d). It may be noted that the phytoplankton biomass was generally well distributed within the upper mixed layer and that the euphotic zone was shallower than this mixed layer (Fig. 4d).

3.2. Communities, absorption and photosynthesis

HPLC derived TChla concentrations were similar at the surface and the SCM for most of the stations, with a maximum of 0.8 mg m^{-3} at 40°E in the core of the eddy (Fig. 5a). Exceptions were noted at 38.7°E, 38.9°E, 40.8°E, and 41°E where TChla was higher at the SCM, and at 40.6°E where TChla was greater at the surface, complementing the fluorescence profiles (Fig. 4d). CHEMTAX revealed that haptophytes were a major component of the biomass across the transect at both the surface and SCM, with diatoms being either dominant or significant contributors between 39.57°E and 41.18°E (Fig. 5b,c). Other groups that were significant on the eastern side of the eddy (41.34°-42.51°E) included *Prochlorococcus*,

pelagophytes and prasinophytes, while on the western boundary, prasinophytes and cryptophytes were prominent (38.90°-39.07°E). To the west of the eddy (38.56°-38.73°E), *Prochlorococcus* was a significant contributor to the pigment biomass, together with haptophytes, *Synechococcus* and prasinophytes (Fig. 5b,c).

There are limitations with CHEMTAX, however, as pigment ratios are influenced by prevailing irradiance and nutrient conditions (Higgins et al., 2011). To minimise the effect of irradiance, surface and SCM samples were analyzed separately. It was more difficult to separate the samples on the basis of nutrients due to the "patchy" variability in the distribution of nitrites (Fig. 4c), and also the requirement to have a sufficient number of samples in each subset to allow for statistical robustness. Variability in nitrogen availability will have an affect on intracellular chlorophyll *a* and therefore on pigment ratios at each station, leading to inaccuracies in estimating the composition of the phytoplankton community (Higgins et al., 2011). An example of such an inaccuracy is the considerably lower chlorophyll *b* output ratios for *Prochlorococcus* relative to the starting ratio (Table 1), most likely leading to an underestimation of the contribution of this group to the community biomass across the eddy.

Phytoplankton specific absorption spectra for 3 localities on the transect are presented in Fig. 6, illustrating the characteristic blue wavelength maximum at 440 nm and red wavelength maximum at 676 nm. The spectra for the surface and the SCM were similar at 40.08°E (eddy core) and at 41.50°E. There were significant differences at 38.73°E, however, where a^*_{ph} at 440 nm was 1.6 times greater at the surface relative to the SCM and this is attributable to the very low TChla (0.127 mg m^{-3}) at the surface at this station ((Fig. 5a). It may also be noted that there was elevated a^*_{ph} around 470 nm and at 640-660 nm compared to the other spectra (Fig. 6).

An example of reconstructed specific absorption spectra for phytoplankton pigments is illustrated in Fig. 7 for the station at 38.73°E to demonstrate the largest contrast between the surface and the SCM. *In vivo*, weight-specific, absorption coefficients are only available for the 13 pigments presented in Fig. 7 and divinyl chlorophyll *b* (Bricaud et al., 2004). Coefficients are not available for chlorophyll c_3, but only for chlorophyll c_1c_2, and the chlorophyll *b* coefficient was used for the collective chlorophyll *b* plus divinyl chlorophyll *b*. Values of a^*_{pig} for monovinyl chlorophyll *a* and chlorophyll c_1c_2 were similar at the surface and SCM, slightly greater at the surface for divinyl chlorophyll *a*, but 3 times greater at the SCM for chlorophyll *b*, particularly at 470 nm and 650 nm (Fig 7a,d). There was also higher a^*_{pig} for 19'-hexanoyloxyfucoxanthin and 19'-butanoyloxyfucoxanthin at the SCM compared to the surface (Fig. 7b,e). In contrast, a^*_{pig} for photoprotective carotenoids was higher at the surface, particularly for zeaxanthin that was the dominant photoprotective carotenoid at 38.73°E (Fig. 7c, f).

There was considerable variability in the phytoplankton specific absorption at 440 nm across the transect (Fig. 8a) that appeared to be related to changes in community composition. The haptophyte, pelagophyte, prasinophyte and cryptophyte proportions in Fig. 5b,c were collectively summed as flagellates, while *Prochlorococcus* and *Synechococcus* were grouped as prokaryotes (Fig 8b,c). The highest values of $a^*_{ph}(440)$ were observed to the west of the eddy and on the boundary (38.56°-38.90°E) where prokaryotes contributed a substantial proportion to the phytoplankton biomass, particularly at the surface. Lowest $a^*_{ph}(440)$ values were estimated where diatoms tended to be dominant (39.57°-41.18°E), while intermediate $a^*_{ph}(440)$ was generally associated with the dominance of flagellates (Fig. 8).

Pigment/TChla ratios were calculated in order to examine phytoplankton acclimation related to accessory chlorophylls, and photosynthetic and photoprotective carotenoids (Fig. 9). Only the most prominent carotenoids were selected and TChlc (total chlorophyll *c*) included chlorophylls c_1,c_2,c_3, MgDVP, $Chlc_2$-MGDG1 and $Chlc_2$-MGDG2 (see Table 1 for pigment names). TChlc was the dominant accessory chlorophyll ratio across the eddy, with peak ratios (~0.5) in the core of the eddy in the vicinity of 40°E (Fig. 9a). DVChla and TChlb ratios were much lower but increased substantially to the west of the eddy as the TChlc ratios decreased. Fucoxanthin dominated the photosynthetic carotenoid ratios over the main part of the eddy (39.40°-41.18°E) but declined on the eastern and western sectors where the 19'-

hexanoylfucoxanthin ratios were mostly higher (Fig. 9b). 19'-Butanoylfucoxanthin ratios were low overall but also increased to the west of the eddy. Ratios for photoprotective carotenoids were low, with diadinoxanthin generally being the main photoprotecting pigment within the eddy and zeaxanthin on the outside, both to the east and west (Fig. 9c). These pigment ratios was mostly similar at the surface and the SCM, although ratios were greater at the surface relative to the SCM at some of the stations. Alloxanthin and ββ -carotene were minor photoprotective pigments, but ββ-carotene ratios were more prominent (Fig. 9d), except at the western boundary of the eddy (39.07°E) where alloxanthin yielded the highest ratios.

Photosynthetic characteristics assessed using active fluorescence indicated a limited range of variability in the absorption cross-section of PSII (σ_{PSII}), although there was more variation at the surface compared to the SCM (Fig. 10a). There was greater variability in the quantum yield of photochemistry in PSII (Fv/Fm) at the surface (0.3-0.53, Fig. 10b) and the pattern along the transect coincided with the surface PAR cycle, where lower Fv/Fm was observed at stations where there was elevated PAR (Fig. 10c). The rate of Q_a reoxidation ($1/\tau_{Qa}$) was highly variable with no distinct differences in the pattern between the surface and the SCM. To the west of the eddy (38.6°–38.7°E), however, $1/\tau_{Qa}$ was significantly greater at the surface relative to the SCM (Fig. 10d).

4. Discussion

Cyclonic eddies have been shown to originate along the eastern boundary of the Mozambique Channel, where they may be formed by turbulence associated with currents interacting with the continental shelf of Madagascar and generally propagating in a southwesterly direction (Halo et al., 2014). Cyclonic eddies can also be generated to the southwest of Madagascar by the friction at the inshore edge of the SEMC as the current flows past the southern tip of Madagascar (de Ruijter et al., 2004; Siedler et al., 2009). The cyclonic eddy in this study was tracked by satellite altimetry prior to the research cruise and appeared to form around 26°S, 43°E and drifted southwest to its location in the northern MB by the time of sampling in mid-July 2013. This cyclonic eddy was unique compared to eddies in the Mozambique Channel (Ternon et al., 2014, Hanke et al., 2014) in that there was a dynamic interaction between the eddy and the SEMC (Fig. 1).

Cyclonic eddies in the Channel were observed to have a distinct deep chlorophyll maximum (DCM), with prokaryotes generally dominating at the surface and flagellates at the DCM (Barlow et al., 2014, Lamont et al., 2014). In contrast, chlorophyll in the MB eddy was distributed throughout the upper 100 m due to the well mixed nature of the upper water column (Fig. 4a,d). TChla was generally similar at the surface and the SCM, except to the west of the eddy where TChla at the SCM was twice that at the surface (Fig 5a). Community structure overall was dominated by haptophytes and diatoms, with diatoms being more prominent in the centre, but *Prochlorococcus* was significant together with haptophytes, pelagophytes, prasinophytes and *Synechococcus* to the west of the eddy (Fig. 5b,c). It is not unusual for diatoms to be prominent in deep sea eddies and Brown et al. (2008) and Rii et al. (2008) also observed diatom prominence in the centre of a Hawaiian cyclonic eddy. These authors speculated that their investigation coincided with an early life cycle stage of the eddy where the physical forces were actively driving upwelling processes in the centre that were conducive to diatom growth. Although there was upward doming of isotherms and nutriclines within the eddy (Figs 3 & 4), the diatoms in the MB eddy most likely originated from the southeast shelf of Madagascar and were transported along the inshore boundary of the SEMC to the eddy. The dynamic interaction between the eddy and the SEMC resulted in the elevated biomass (Figs. 1b & 2c) most likely containing the diatoms being entrained into the cyclonic flow of the eddy and concentrated towards the centre (Fig. 5b,c). It may be noted that the western boundary of the eddy was dominated by haptophytes (Fig. 5b,c). There appeared to be sufficient nutrients to sustain the populations due to the mixed layer reaching the nutriclines at 80-100 m (Fig. 4), presumably driven by the wind regime over the eddy. Although they were low in the upper 100 m, silicate and phosphate levels (data not shown) did not appear to be limiting, and while nitrates were generally below detection limit (Fig. 4b), nitrite was available (Fig. 4c).

Considering that Z_e was shallower than Z_m (Fig. 4), the question arises as to the acclimation of the communities to changing irradiance across the eddy. The a^*_{ph} spectra in Fig. 6 suggests that there were only small differences in a^*_{ph} between the surface and SCM at most of the stations, but outside the eddy at 38.73°E there were significant differences, with surface a^*_{ph} at blue wavelengths being greater due to very low TChla (Fig. 6). Absorption coefficients determined by QFT yields the 'packaged' absorption of the phytoplankton community, whereas the reconstructed spectra of pigments is the 'unpackaged' absorption that does not account for the 'packaging' of pigments within the protein-pigment complexes in phytoplankton cells (Johnsen et al., 2011). Nevertheless, spectral reconstruction can convey information concerning the role of accessory pigments in light absorption. In the Sargasso Sea, Bidigare et al. (1992) noted that accessory pigments accounted for 60% of the light absorbed at the surface and 90% at the base of the euphotic zone. Barlow et al. (2013) observed that the proportion of irradiance absorbed by photosynthetic carotenoids and chlorophyll *c* increased as light decreased in mixed diatom-flagellate communities on the east coast of South Africa, while there was a high proportion of photoprotective carotenoid absorption at the surface.

At 38.73°E, the phytoplankton comprised *Prochlorococcus* and various flagellates (Fig. 5) and the reconstructed pigment spectra revealed particularly high a^*_{pig} by chlorophyll *b* at 470 nm and 650 nm at the SCM relative to the surface (Fig. 7), explaining the elevated a^*_{ph} around 470 nm and at 640-660 nm in Fig. 6. The HPLC method does not separate monovinyl and divinyl chlorophyll *b* and so the chlorophyll *b* absorption can be attributed to absorption by both divinyl chlorophyll *b* in *Prochlorococcus* and monovinyl chlorophyll *b* in prasinophytes. Haptophytes and pelagophytes were also present at 38.73°E, particularly at the SCM (Fig. 5), and consequently there was elevated a^*_{pig} at blue-green wavelengths by 19'-hexanoyloxyfucoxanthin and 19'-butanoyloxyfucoxanthin at the SCM (Fig. 7). In contrast, a^*_{pig} by zeaxanthin was greater at the surface (Fig. 7) and this may be attributed to an increase in this pigment to perform photoprotection by *Prochlorococcus*, and Synechococcus (Fig. 5b). There are two distinct ecotypes of *Prochlorococcus*, one adapted to high light conditions and the other to low light (Bouman et al., 2011). The low-light strains are well adapted to low irradiance conditions and the spectral quality of the subsurface light field, and a high proportion of divinyl chlorophyll *b* in some strains allows these cells to absorb more low intensity blue light near the base of the euphotic zone (Moore et al., 1995), thus conferring an advantage for growth deep in the water column. A low-light strain was therefore probably present at the SCM at 38.73°E in July 2013 since a^*_{pig} indicated such absorption characteristics. *Prochlorococcus* has a very high efficiency for absorption as its minute size results in a lowered light scattering efficiency and high pigment content per cell (Morel et al., 1993). Thus *Prochlorococcus* is rather unique in that the probability for photons to be absorbed is greater than that of being scattered.

Specific absorption at 440 nm indicated small differences in a^*_{ph} between the surface and SCM (Fig. 8a), confirming that strong mixing was prevalent in the Z_m over most of the transect. At 38.56°-39.07°E, $a^*_{ph}(440)$ was greater at the surface than the SCM (Fig. 8a), suggesting that mixing was perhaps weaker on the western side of the eddy where Z_e tended to be deeper (Fig. 4). Values of $a^*_{ph}(440)$ were ~0.05 m^2 mg^{-1} where diatoms were dominant, 0.06-0.11 m^2 mg^{-1} for the flagellates and >0.11 m^2 mg^{-1} for prokaryote dominance (Fig 8). These values are comparable with studies in the Mozambique Channel that indicated $a^*_{ph}(440)$ of 0.03-0.05 m^2 mg^{-1} for diatom dominated communities, 0.05-0.14 m^2 mg^{-1} for flagellates, and 0.13-0.2 m^2 mg^{-1} for prokaryote domination (Barlow et al., 2008, 2014). Other investigations showed a greater variability of 0.05-0.1 m^2 mg^{-1} for diatom $a^*_{ph}(440)$ in an inshore shelf ecosystem influenced by the Agulhas Current (Barlow et al., 2013) that may be a reflection of varying sizes of coastal diatoms. Studies in the northwest Indian Ocean demonstrated that $a^*_{ph}(440)$ was 0.03-0.05 m^2 mg^{-1} in the Red Sea where large diatoms were prominent, 0.06-0.12 m^2 mg^{-1} in the Gulf of Aden and the Somali Current where *Synechococcus* and *Prochlorococcus* were numerically dominant (Sathyendranath et al., 1996). For the Arabian Sea, Sathyendranath et al. (1999) reported $a^*_{ph}(440)$ for communities dominated by diatoms to be 0.048-0.071 m^2 mg^{-1}, while in small-celled prokaryote communities $a^*_{ph}(440)$ was 0.124. The variability in specific absorption in these collective studies reflects differences in pigment packaging and pigment content (Kirk, 1994) between components of the phytoplankton communities in the southwestern and northwestern Indian Ocean. Microphytoplankton

such as diatoms usually have a high pigment content per cell and greater packaging, leading to low $a^*_{ph}(440)$ values (Bricaud et al., 2004). Picophytoplankton such as prokaryotes, on the other hand, have considerably less pigment per cell but no or minimal packaging yielding high $a^*_{ph}(440)$ values, while flagellate cells (nanophytoplankton) have intermediate pigment content and packaging and specific absorption (Bricaud et al., 2004).

Photosynthetic pigment:TChla ratios were very similar at the surface and SCM across the eddy (Fig. 9a,b), providing further evidence for strong mixing in the upper water column, with TChlc, fucoxanthin and 19'-hexanoyloxyfucoxanthin ratios generally varying according to the change in phytoplankton biomass and community composition (Fig. 5). It may be noted that TChlc ratios were of a similar magnitude to those of fucoxanthin, suggesting that the various chlorophyll *c*'s played an important role in the absorption of light for community photosynthesis under the fluctuating light regime induced by mixing, particularly at blue wavelengths (Fig 7a,d). The higher 19'-hexanoyloxyfucoxanthin ratios in the eastern and western sectors coincided with greater proportions of haptophytes in the community (Fig 5) and, together with fucoxanthin and 19'-butanoyloxyfucoxanthin, these carotenoids optimised absorption of light in the blue-green wavelength range of 480-520 nm (Fig, 7b,e). Experiments simulating fluctuating light regimes between low and high irradiances with various algal cultures showed that pigment:TChla ratios varied only slightly compared to ratios for species grown under constant low light (Nicklisch and Woitke, 1999; Fietz and Nicklisch, 2002). It may be speculated therefore that exposure to fluctuating light by the communities in the MB eddy induced an overall acclimation strategy to relatively low light conditions. To the west of the eddy, the ratios for the divinyl chlorophylls were greater than those for the photosynthetic carotenoids, particularly for TChlb at the SCM at 38.73^{o}E (Fig. 9a,b), and this may have reflected a high content of divinyl chlorophyll pigments in *Prochlorococcus* cells. It was suggested above that there was reduced mixing to the west of the eddy, leading to a deeper SCM, and the high TChlb ratio at the SCM therefore indicated photoacclimation by the low-light ecotype of *Prochlorococcus* (divinyl chlorophyll *b*), but also by prasinophytes (chlorophyll *b*) that were prominent at the SCM at 38.73^{o}E (Fig. 5c).

Although photoprotective pigment:TChla ratios were low, an interesting observation is that diadinoxanthin was the main photoprotective carotenoid within the eddy, while zeaxanthin was dominant outside the eddy and at the boundaries (Fig. 9c,d). Diadinoxanthin is a protecting pigment in diatoms and haptophytes and zeaxanthin performs this role in prokaryotes (Brunet et al., 2011). *Prochlorococcus* was prominent in the community to the east and west of the eddy (Fig. 5), and it seems that these small cells were more efficient in synthesizing elevated levels of zeaxanthin compared to diadinoxanthin synthesis in the eukaryotes. Diadinoxanthin seemed to exhibit a diel response as the ratio was higher under elevated PAR during daylight hours (grey shaded areas in Fig. 9c) and lower at night. There appeared to be no similar diel changes in the ratios for alloxanthin and β,β-carotene, except at 39.07^{o}E, where alloxanthin ratios were high at midday (Fig 9d) due to the higher proportion of cryptophytes in the community at this locality (Fig. 5b,c).

The photosynthetic performance indicated that, physiologically, the community was not nutrient stressed as Fv/Fm values were >0.3 along the transect (Fig 10). In nutrient stressed cells, Fv/Fm is usually <0.3 as observed by Painter et al., (2010) in phytoplankton in the northeast Atlantic. While no particular pattern could be discerned for the absorption cross-section of PSII (σ_{PSII}), Fv/Fm appeared to respond to the diel irradiance cycle by decreasing during the day under elevated PAR, particularly at the surface (Fig. 10b,c). Nutritional state and community composition strongly influence Fv/Fm values (Suggett et al., 2009), but this is not likely to be the case in this study as there was a consistent phytoplankton community that was not nutrient stressed. The reduced quantum efficiency of photochemistry in PSII (Fv/Fm) under high light during the day in the MB eddy may be attributed to photoinhibition in PSII (Oquist et al., 1992), as also observed by Schuback et al. (2016) in phytoplankton in the northeast subarctic Pacific. A diel cycle in the rate of Q_a reoxidation ($1/\tau_{Qa}$) was noted by Schuback et al. (2016), with a light-dependent increase in $1/\tau_{Qa}$, while Moore et al. (2006) demonstrated an increase in the rate of whole-chain electron transfer during the day. There was no similar discernable light-dark pattern in $1/\tau_{Qa}$ for the MB eddy community

as $1/\tau_{Qa}$ was highly variable (Fig. 10d). The observed pattern may be a reflection of the photosynthetic response by the phytoplankton to rapidly fluctuating light conditions as they were mixed in the water column. The flagellate-*Prochlorococcus* community to the west of the eddy (38.6°–38.7°E) had high values of $1/\tau_{Qa}$ at the surface, however, suggesting faster flow of electrons downstream from Q_a. This may have served as a photoprotective mechanism through upregulation of alternative electron sinks (Mackey et al., 2008), but sampling at 38.73°E was undertaken in the dark and not during maximum PAR at midday. *Prochlorococcus* was a significant component of the community, though, and since these small cells have a very high efficiency for light absorption (Morel et al., 1993) that drives photosynthesis and electron transport, the elevated $1/\tau_{Qa}$ may have reflected the potential for fast electron flow downstream of PSII even in the dark.

In summary, this study demonstrated that a diatom-flagellate community within a cyclonic eddy was well acclimated to fluctuating light conditions due to strong mixing in the eddy, since there was generally little difference in population structure, absorption characteristics and pigment:TChla ratios between the surface and the SCM. There was an increase in diadinoxanthin:TChla ratios and a decline in the quantum efficiency of photochemistry in PSII under high light conditions, however, indicating some photoinhibition at the surface even in a well mixed environment. A flagellate-*Prochlorococcus* population outside the eddy displayed different characteristics, with elevated specific absorption and divinyl chlorophyll *a*, chlorophyll *b* and 19'-hexanoyloxyfucoxanthin ratios at the SCM, reflecting acclimation to low irradiance blue light to maintain photosynthesis at depth. But elevated zeaxanthin ratios and a higher rate of Q_a reoxidation indicated that the surface community was well primed for photoprotection under high irradiance conditions.

Acknowledgements

We sincerely thank the officers and crew of the RV *Algoa* for their skilled cooperation and assistance during the cruise; D Walker and C Niewenhuys for shipboard technical support; H Ismail for nutrient analysis; the African Coelacanth Ecosystem Programme (ACEP), the South African National Research Foundation and Department of Environmental Affairs for funding support. Satellite altimetry products were produced by Ssalto/Duacs and distributed by AVISO with support from CNES (http://www.aviso.oceanobs.com/). Satellite data from the MODIS Aqua sensor were processed by the Ocean Biology Processing Group at NASA's Goddard Space Flight Centre (http://oceancolor.gsfc.nasa.gov).

References

Barlow, R., Kyewalyanga, M., Sessions, H., van den Berg, M., Morris, T., 2008. Phytoplankton pigments, functional types, and absorption properties in the Delagoa and Natal Bights of the Agulhas ecosystem. Est. Coast. Shelf Sc. 80, 201-211.

Barlow, R., Lamont, T., Britz, K., Sessions, H., 2013. Mechanisms of phytoplankton adaptation to environmental variability in a shelf ecosystem. Est. Coast. Shelf Sc. 133, 45–57.

Barlow, R., Lamont, T., Morris, T., Sessions. H., van den Berg, M., 2014. Adaptation of phytoplankton communities to mesoscale eddies in the Mozambique Channel. Deep-Sea Res. II 100, 106-114.

Bricaud, A., Claustre, H., Ras, J., Oubelkheir, K., 2004. Natural variability of phytoplanktonic absorption in oceanic waters: influence of the size structure of algal populations. J. Geophys. Res. 109, C11010.

Bricaud, A., Stramski, D., 1990. Spectral absorption coefficients of living phytoplankton and nonalgal biogenous matter: a comparison between the Peru upwelling area and the Sargasso Sea. Limnol. Oceanogr. 35, 562-582.

Bidigare, R., Prezelin, B., Smith, R., 1992. Bio-optical models and the problem of scaling. In: Falkowski, P., Woodhead, A. (Eds.), Primary productivity and biogeochemical cycles in the Sea. Plenum Press, New York, pp. 175-212.

Bouman, H., Ulloa, O., Barlow, R., Li, W., Platt, T., Zwirglmaier, K., Scanlan, D., Sathyendranath, S., 2011. Water-column stratification governs the community structure of subtropical marine picophytoplankton. Environ. Microbiol. Rep. 3, 473-482.

Brown, S., Landry, M., Selph, K., Jin Yang, E., Rii, Y., Bidigare, R., 2008. Diatoms in the desert: Plankton community response to a mesoscale eddy in the subtropical North Pacific. Deep-Sea Res. II 55, 1321-1333.

Brunet, C., Johnsen, G., Lavaud, J., Roy, S., 2011. Pigments and photoacclimation processes. In: Roy, S., Llewellyn, C., Egeland, E., Johnsen, G. (Eds.) Phytoplankton pigments: Characterization, chemotaxonomy and applications in oceanography. Cambridge University Press, Cambridge, pp. 445-471.

Cleveland, J., Weidemann, A., 1993. Quantifying absorption by aquatic particles: a multiple scattering correction for glass-fibre filters. Limnol. Oceanogr. 38, 1321-1327.

De Ruijter, W., van Aken, H., Beier, E., Lutjeharms, J., Matano, R., Schouten, M., 2004. Eddies and dipoles around South Madagascar: formation, pathways and large-scale impact. Deep-Sea Res. I 51, 383-400.

De Ruijter, W., Ridderinkhof, H., Schouten, M., 2005. Variability of the southwest Indian Ocean. Phil. Trans. Royal Soc. 363, 63–76.

Duncan, C., 1970. The Agulhas Current. PhD thesis, Univ. Hawaii, 76 pp.

Fietz, S., Nicklisch, A., 2002. Acclimation of the diatom *Stephanodiscus neoastraea* and the cyanobacterium *Planktothrix agardhii* to simulated natural light fluctuations. Photosyn. Res. 72, 95-106.

Gorbunov, M., Falkowski, P., 2004. Fluorescence induction and relaxation (FIRe) technique and instrumentation for monitoring photosynthetic processes and primary production in aquatic ecosystems. In: Bruce, D., van der Est, A. (Eds.) Photosynthesis: Fundamental aspects to global perspectives. Allen Press, Montreal, pp. 1029-1031.

Grundlingh, M., (1985) Features of the circulation in the Mozambique Basin in 1981. J. Mar. Res. 43, 779-792.

Grundlingh, M., Carter, R., Stanton, R., 1991. Circulation and water properties of the Southwest Indian Ocean, Spring 1987. Prog. Oceanogr. 28, 305-342.

Halo, I., Backeberg, B., Penven, P., Ansorge, I., Reason, C., Ullgren, J., 2014. Eddy properties in the Mozambique Channel: a comparison between observations and two numerical ocean circulation models. Deep-Sea Res. II 100, 38-53.

Hancke, L., Roberts, M., Ternon, J-F., 2014. Surface drifter trajectories highlight flow pathways in the Mozambique Channel. Deep-Sea Res. II 100, 27-37.

Hickman, A., Holligan, P., Moore, M., Sharples, J., Krivtsov, V., Palmer, M., 2009. Distribution and chromatic adaptation of phytoplankton within a shelf sea thermocline. Limnol. Oceanogr. 54, 525–536.

Higgins, H., Wright, S., Schluter, L., 2011. Quantitative interpretation of chemotaxonomic pigment data. In: Roy, S., Llewellyn, C., Egeland, E., Johnsen, G. (Eds.) Phytoplankton pigments: Characterization, chemotaxonomy and applications in oceanography. Cambridge University Press, Cambridge, pp. 257-313.

IOC, SCOR, IAPSO, 2010. The international thermodynamic equation of seawater-2010. Calculation and use of thermodynamic properties. Intergovernmental Oceanographic Commission, Manuals and Guides No. 56, UNESCO (English), 196 pp. Available online at http://www.teos-10.org/pubs/TEOS-10_Manual.pdf.

Jeffrey, S., Wright, S., Zapata, M., 2011. Microalgal classes and their signature pigments. In: Roy, S., Llewellyn, C., Egeland, E., Johnsen, G. (Eds.) Phytoplankton pigments: characterization, chemotaxonomy and applications in oceanography. Cambridge University Press, Cambridge, pp. 3-77.

Johnsen, G., Bricaud, A., Nelson, N., Prezelin, B., Bidigare, R., 2011. In vivo bio-optical properties of phytoplankton pigments. In: Roy, S., Llewellyn, C., Egeland, E., Johnsen, G. (Eds.) Phytoplankton pigments: characterization, chemotaxonomy and applications in oceanography. Cambridge University Press, Cambridge, pp. 496-537.

Kirk, J., 1994. Light and Photosynthesis in Aquatic Ecosystems, 2nd Edition. Cambridge University Press, Cambridge, 509pp.

Kolber, Z., Prásil, O., Falkowski, P., 1998. Measurements of variable chlorophyll fluorescence using fast repetition techniques: defining methodology and experimental protocols. Biochim. Biophys. Acta 1367, 88-106.

Lamont, T., Barlow, R., Morris, T., van den Berg, M., 2014. Characterisation of mesoscale features and phytoplankton variability in the Mozambique Channel. Deep-Sea Res. II 100, 94-105.

Mackey, M., Mackey, D., Higgins, H., Wright, S., 1996. CHEMTAX- a program for estimating class abundances from chemical markers: application to HPLC measurements of phytoplankton. Mar. Ecol. Prog. Ser. 144, 265–283.

Mackey, K., Paytan, A., Grossman, A., Bailey, S., 2008. A photosynthetic strategy for coping in a high-light, low-nutrient environment. Limnol. Oceanogr. 53, 900–913.

Mitchell, B., Kiefer, D., 1988. Chlorophyll *a* specific absorption and fluorescence excitation spectra for light-limited phytoplankton. Deep-Sea Res. 35, 639-663.

Moore, L., Goericke, R., Chisholm, S., 1995. Comparative physiology of *Synechococcus* and *Prochlorococcus*: influence of light and temperature on growth, pigments, fluorescence and absorptive properties. Mar. Ecol. Prog. Ser. 116, 259-275.

Moore, C., Suggett, D., Hickman, A., Kim, Y-N., Tweddle, J., Sharples, J., Geider, R., Holligan, P., 2006. Phytoplankton photoacclimation and photoadaptation in response to environmental gradients in a shelf sea. Limnol. Oceanogr. 51, 936–949.

Morel, A., Ahn, Y-H., Partensky, F., Vaulot, D., Claustre, H., 1993. *Prochlorococcus* and *Synechococcus*: a comparative study of their optical properties in relation to their size and pigmentation. J. Mar. Res. 51, 617-649.

Morel, A., Berthon, J-F., 1989. Surface pigments, algal biomass profiles, and the potential production of the euphotic layer: relationships reinvestigated in view of remote sensing applications. Limnol. Oceanogr. 34, 1545–1562.

Morel, A., Maritorena, S., 2001. Bio-optical properties of oceanic waters: a reappraisal. J. Geophys. Res. 106 (C4), 7163-7180.

Mostert, S., 1983. Procedures used in South Africa for the automatic photometric determination of micronutrients in seawater. S. Afr. J. Mar. Sci. 1, 189–198.

Nicklisch, A., Woitke, P., 1999. Pigment content of selected planktonic algae in response to simulated natural light fluctuations and a short photoperiod. Internat. Rev. Hydrobiol. 84, 479-495.

Öquist, G., Chow, W., Anderson, J., 1992. Photoinhibition of photosynthesis represents a mechanism for the long-term regulation of photosystem II. Planta 186, 450-460.

Painter, S., Lucas, M., Stinchcombe, M., Bibby, T., Poulton, A., 2010. Summertime trends in pelagic biogeochemistry at the porcupine Abyssal Plain study site in the northeast Atlantic. Deep-Sea Res. II 57, 1313-1323.

Ridderinkhof, W., Le Bars, D., von der Heydt, A., de Ruijter, W., 2013. Dipoles of the South East Madagascar Current. Geophys. Res. Lett. 40, 558-562.

Rii, Y., Brown, S., Nencioli, F., Kuwahara, V., Dickey, T., Karl, D., Bidigare, R., 2008. The transient oasis: nutrient-phytoplankton dynamics and particle export in Hawaiian lee cyclones. Deep-Sea Res. II 55, 1275-1290.

Roesler, C. 1998. Theoretical and experimental approaches to improve the accuracy of particulate absorption coefficients derived from the quantitative filter technique. Limnol. Oceanogr. 43, 1649-1660.

Sathyendranath, S., Platt, T., Stuart, V., Irwin, B., Veldhuis, M., Kraay G., Harrison. W., 1996. Some bio-optical characteristics of phytoplankton in the NW Indian Ocean. Mar. Ecol. Prog. Ser. 132, 299-311.

Sathyendranath, S., Stuart, V., Irwin, B., Maass, H., Savidge, G., Gilpin, L., Platt, T., 1999, Seasonal variations in bio-optical properties of phytoplankton in the Arabian Sea. Deep-Sea Res. II 46, 633-653.

Schouten, M., de Ruijter, W., van Leeuwen. P., 2002. Upstream control of Agulhas ring shedding. J. Geophys. Res. 107 (C8), 3109–3120.

Schuback, N., Flecken, M., Maldonado, M., Tortell, P., (2016) Diurnal variation in the coupling of photosynthetic electron transport and carbon fixation in iron-limited phytoplankton in the NE subarctic Pacific. Biogeosci. 13, 1019-1035.

Siedler, G., Rouault, M., Biastoch, A., Backeberg, B., Reason, C., Lutjeharms, J., 2009. Modes of the southern extension of the East Madagascar Current. J. Geophys. Res. 114, C01005.

Suggett, D., Moore, C., Hickman, A., Geider, R., 2009. Interpretation of fast repetition rate (FRR) fluorescence: signatures of phytoplankton community structure versus physiological state. Mar. Ecol. Prog. Ser. 376, 1-19.

Tassan, S., Ferrari, G., 1995. An alternative approach to absorption measurements of aquatic particles retained on filters. Limnol. Oceanogr. 40, 1358-1368.

Ternon, J-F., Roberts, M., Morris, T., Hanke, L., Backeberg, B., 2014. In situ measured current structures of the eddy field in the Mozambique Channel. Deep-Sea Res. II 100, 10-26.

Thomson, R., Fine, I., 2003. Estimating mixed layer depth from oceanic profile data. J. Atmos. Oceanic Technol. 20, 319-329.

Van Heukelem, L., Hooker, S., 2011. The importance of a quality assurance plan for method validation and minimizing uncertainties in the HPLC analysis of phytoplankton pigments. In: Roy, S., Llewellyn, C., Egeland, E., Johnsen, G. (Eds.) Phytoplankton pigments: characterization, chemotaxonomy and applications in oceanography. Cambridge University Press, Cambridge, pp. 195-242.

Wright, S., Ishikawa, A., Marchant, H., Davidson, A., van den Enden, R., Nash, G., 2009. Composition and significance of picophytoplankton in Antarctic waters. Pol. Biol. 797–808.

Wyrtki, K., 1971. Oceanographic atlas of the International Indian Ocean Expedition. Nat. Sci. Found., Washington, 531 pp.

Zapata, M., Rodríguez, F., Garrido, J., 2000. Separation of chlorophylls and carotenoids from marine phytoplankton: a new HPLC method using a reversed phase C8 column and pyridine containing mobile phases. Mar. Ecol. Prog. Ser. 195, 29-45.

Zhu, Y., Ishizaka, J., Tripathy, S., Wang, S., Mino, Y., Matsuno, T.,·Suggett, D., 2016. Variation of the photosynthetic electron transfer rate and electron requirement for daily net carbon fixation in Ariake Bay, Japan. J. Oceanogr. doi: 10.1007/s10872-016-0370-4.

Table 1

Pigment:chlorophyll *a* starting and output ratios in the CHEMTAX analysis of HPLC pigments. Starting ratios derived from Higgins et al. (2011). Chla-chlorophyll *a*; DVChla-divinyl chlorophyll *a*; Chlb-chlorophyll *b*+ divinyl chlorophyll *b*; MgDVP-Mg-2,4-dininyl pheoporphyrin a_5 monomethyl ester; Chlc1-chlorophyll c_1; Chlc2-chlorophyll c_2; Chlc3-chlorophyll c_3; Per-peridinin; But-19'-butanoyloxyfucoxanthin; Fuc-fucoxanthin; Neo-neoxanthin; Viol-violaxanthin; Pras-prasinoxanthin; Hex-19'-hexanoyloxyfucoxanthin; Allo-alloxanthin; Zea-zeaxanthin; Anth-antheraxanthin; Asta-astaxanthin; Lut-lutein; Chlc2-MGDG1-chlorophyll c_2-monogalactosyldiacylglyceride ester [18:4/14:0]; Chlc2-MGDG2- chlorophyll c_2-monogalactosyldiacylglyceride ester [14:0/14:0].

Group	Chla	DV Chla	Chlb	Mg DVP	Chlc1	Chlc2	Chlc3	Per	But	Fuc	Neo	Viol	Pras	Hex	Allo	Zea	Anth	Asta	Lut	Chlc2-MG DG1	Chlc2-MG DG2
Starting Ratios																					
Diatoms-1	1	0	0	0	0.087	0.18	0	0	0	0.775	0	0	0	0	0	0	0	0	0	0	0
Diatoms-2	1	0	0	0	0	0.284	0.083	0	0	0.998	0	0	0	0	0	0	0	0	0	0	0
Dinoflagellates	1	0	0	0.006	0	0.22	0	0.56	0	0	0	0	0	0	0	0	0	0	0	0	0
Cryptophytes	1	0	0	0	0	0.2	0	0	0	0	0	0	0	0	0.38	0	0	0	0	0	0
Pelagophytes	1	0	0	0	0.01	0.275	0.23	0	0.66	0.78	0	0	0	0	0	0	0	0	0	0	0
Haptophytes	1	0	0	0.009	0	0.21	0.18	0	0.04	0.31	0	0	0	0.47	0	0	0	0	0	0.09	0.103
Prasinophytes-1	1	0	0.631	0.008	0	0	0	0	0	0	0.072	0.138	0	0	0	0.026	0.023	0	0.057	0	0
Prasinophytes-3	1	0	0.73	0.062	0	0	0	0	0	0	0.063	0.054	0.25	0	0	0.058	0.021	0	0.021	0	0
Chlorophytes	1	0	0.32	0	0	0	0	0	0	0	0.066	0.049	0	0	0	0.032	0.014	0.012	0.17	0	0
Cyanobacteria (Synechococcus)	1	0	0	0	0	0	0	0	0	0	0	0	0	0	0	0.64	0	0	0	0	0
Prochlorococcus	0	1	0.99	0	0	0	0	0	0	0	0	0	0	0	0	0.39	0	0	0	0	0
Surface																					
Diatoms-1	1	0	0	0	0.108	0.168	0	0	0	0.669	0	0	0	0	0	0	0	0	0	0	0
Diatoms-2	1	0	0	0	0	0.253	0.183	0	0	0.681	0	0	0	0	0	0	0	0	0	0	0
Dinoflagellates	1	0	0	0.004	0	0.172	0	0.685	0	0	0	0	0	0	0	0	0	0	0	0	0
Cryptophytes	1	0	0	0	0	0.208	0	0	0	0	0	0	0	0	0.347	0	0	0	0	0	0
Pelagophytes	1	0	0	0	0.008	0.329	0.278	0	0.706	0.561	0	0	0	0	0	0	0	0	0	0	0
Haptophytes	1	0	0	0.010	0	0.087	0.155	0	0.046	0.207	0	0	0	0.476	0	0	0	0	0	0.063	0.061
Prasinophytes-1	1	0	0.727	0.007	0	0	0	0	0	0	0.056	0.121	0	0	0	0.018	0.023	0	0.060	0	0
Prasinophytes-3	1	0	0.714	0.067	0	0	0	0	0	0	0.072	0.069	0.126	0	0	0.040	0.027	0	0.016	0	0
Chlorophytes	1	0	0.245	0	0	0	0	0	0	0	0.087	0.039	0	0	0	0.027	0.017	0.015	0.183	0	0
Cyanobacteria (Synechococcus)	1	0	0	0	0	0	0	0	0	0	0	0	0	0	0	0.696	0	0	0	0	0
Prochlorococcus	0	1	0.385	0	0	0	0	0	0	0	0	0	0	0	0	0.360	0	0	0	0	0
Sub-Surface																					
Diatoms-1	1	0	0	0	0.097	0.180	0	0	0	0.526	0	0	0	0	0	0	0	0	0	0	0
Diatoms-2	1	0	0	0	0	0.257	0.119	0	0	0.742	0	0	0	0	0	0	0	0	0	0	0
Dinoflagellates	1	0	0	0.004	0	0.286	0	0.685	0	0	0	0	0	0	0	0	0	0	0	0	0
Cryptophytes	1	0	0	0	0	0.156	0	0	0	0	0	0	0	0	0.275	0	0	0	0	0	0
Pelagophytes	1	0	0	0	0.011	0.196	0.165	0	0.822	0.659	0	0	0	0	0	0	0	0	0	0	0
Haptophytes	1	0	0	0.008	0	0.131	0.242	0	0.028	0.220	0	0	0	0.492	0	0	0	0	0	0.073	0.058
Prasinophytes-1	1	0	0.805	0.010	0	0	0	0	0	0	0.084	0.127	0	0	0	0.022	0.018	0	0.072	0	0
Prasinophytes-3	1	0	0.913	0.074	0	0	0	0	0	0	0.047	0.047	0.197	0	0	0.049	0.026	0	0.018	0	0
Chlorophytes	1	0	0.430	0	0	0	0	0	0	0	0.075	0.058	0	0	0	0.023	0.011	0.012	0.135	0	0
Cyanobacteria (Synechococcus)	1	0	0	0	0	0	0	0	0	0	0	0	0	0	0	0.557	0	0	0	0	0
Prochlorococcus	0	1	0.619	0	0	0	0	0	0	0	0	0	0	0	0	0.257	0	0	0	0	0

Figure legends

Fig. 1. (a) Sea Surface Height (colour contours) and geostrophic velocity (black arrows) on 17 July 2013, and (b) MODIS Aqua chlorophyll *a* concentration for 12-19 July 2013 over the Mozambique Basin. Black boxes highlight the location of the eddy and white and black dots indicate positions of the sampling stations. White areas indicate missing data due to cloud cover.

Fig. 2. Sea Surface Height (colour contours) and geostrophic velocity (black arrows) within the black box of Fig. 1a for (a) 17 July 2013 and (b) 22 July 2013, and MODIS chlorophyll *a* within the black box of Fig. 1b for (c) 12-19 July 2013 and (d) 20-27 July 2013. White and black dots indicate positions of the sampling stations. White areas indicate missing data due to cloud cover.

Fig. 3. Vertical section of conservative temperature through the cyclonic eddy transect. The black dashed line highlights the 9^{o}C isotherm and the solid black line indicates the depth of the upper mixed layer (Z_m).

Fig. 4. Vertical sections of (a) conservative temperature, (b) nitrate concentration, (c) nitrite concentration, and (d) chlorophyll *a* concentration estimated from the CTD fluorescence profiles. Black dots indicate location of surface samples and white dots indicate depths of SCM samples. The black dashed line indicates the depth of the euphotic zone (Z_e) and the upper mixed layer ($Z_{m)}$ by the solid black line.

Fig. 5. Distribution pattern of (a) TChla at the surface (Surf) and the sub-surface chlorophyll maximum (SCM) and the proportion of each phytoplankton group contributing to TChla at (b) the surface and (c) the SCM. Vertical dashed lines indicate the boundaries of the eddy.

Fig. 6. Phytoplankton chlorophyll-specific absorption spectra (a^*_{ph}) at the surface and the SCM for 3 selected stations on the eddy transect.

Fig. 7. Reconstructed specific absorption spectra for 13 selected pigments (a^*_{pig}) for (a, b, c) the surface and (d, e, f) the SCM at 38.73^{o}E. Chlorophyll spectra are presented in (a) and (d), photosynthetic carotenoids in (b) and (e) and photoprotective carotenoids in (c) and (f). MVChla-monovinyl chlorophyll *a*; DVChla-divinyl chlorophyll *a*; Chlb-chlorophyll *b* + divinyl chlorophyll *b*; Chlc-chlorophyll c_1,c_2; a-Carotene-β,ε-carotene; B-Carotene-β,β-carotene.

Fig. 8. Distribution pattern of phytoplankton specific absorption at 440 nm [a^*_{ph} (440)] at (a) the surface and the SCM, and the proportion of diatoms, dinoflagellates, flagellates and prokaryotes contributing to TChla at (b) the surface and (c) the SCM. Vertical dashed lines indicate the boundaries of the eddy.

Fig. 9. Distribution pattern of selected pigment/TChla ratios at the surface and the SCM for (a) accessory chlorophylls, (b) photosynthetic carotenoids and (c, d) photoprotective carotenoids. The maximum zeaxanthin/TChla ratio at the surface is indicated as 0.35. Grey shaded areas in (c, d) indicate elevated PAR during daylight hours. Vertical dashed lines designate the boundaries of the eddy. DVChla-divinyl chlorophyll *a*; TChlb-chlorophyll *b*+divinyl chlorophyll *b*; TChlc-chlorophylls c_1,c_2,c_3+MgDVP+Chlc$_2$-MGDG1+Chlc$_2$-MGDG2; But'fuco-19'-butanoyloxyfucoxanthin; Hex'fuco-19'-hexanoyloxyfucoxanthin; Fuco-fucoxanthin; Diad-diadinoxanthin; Zea-zeaxanthin; Allo-alloxanthin; B-Caro-β,β-carotene.

Fig. 10. Distribution pattern of (a) $\sigma_{PSII,452}$, (b) Fv/Fm, (c) PAR and (d) $1/\tau_{Qa}$ at the surface and SCM. Vertical dashed lines indicate the boundaries of the eddy.

Fig. 1

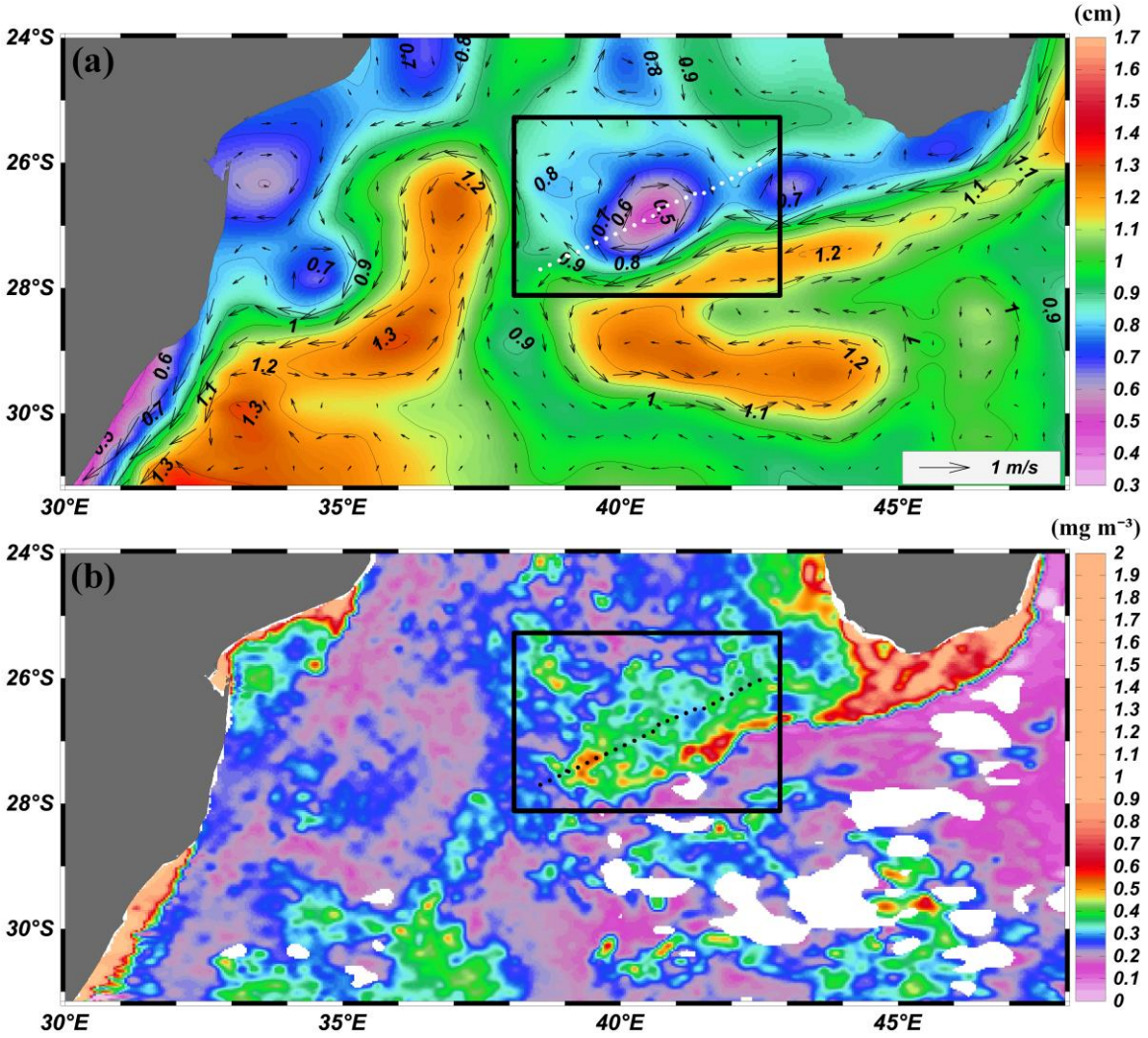
(a)
(cm)
1.7
1.6
1.5
1.4
1.3
1.2
1.1
1
0.9
0.8
0.7
0.6
0.5
0.4
0.3
1 m/s
24°S
26°S
28°S
30°S
30°E
35°E
40°E
45°E
(b)
(mg m⁻³)
2
1.9
1.8
1.7
1.6
1.5
1.4
1.3
1.2
1.1
1
0.9
0.8
0.7
0.6
0.5
0.4
0.3
0.2
0.1
0

Fig. 2

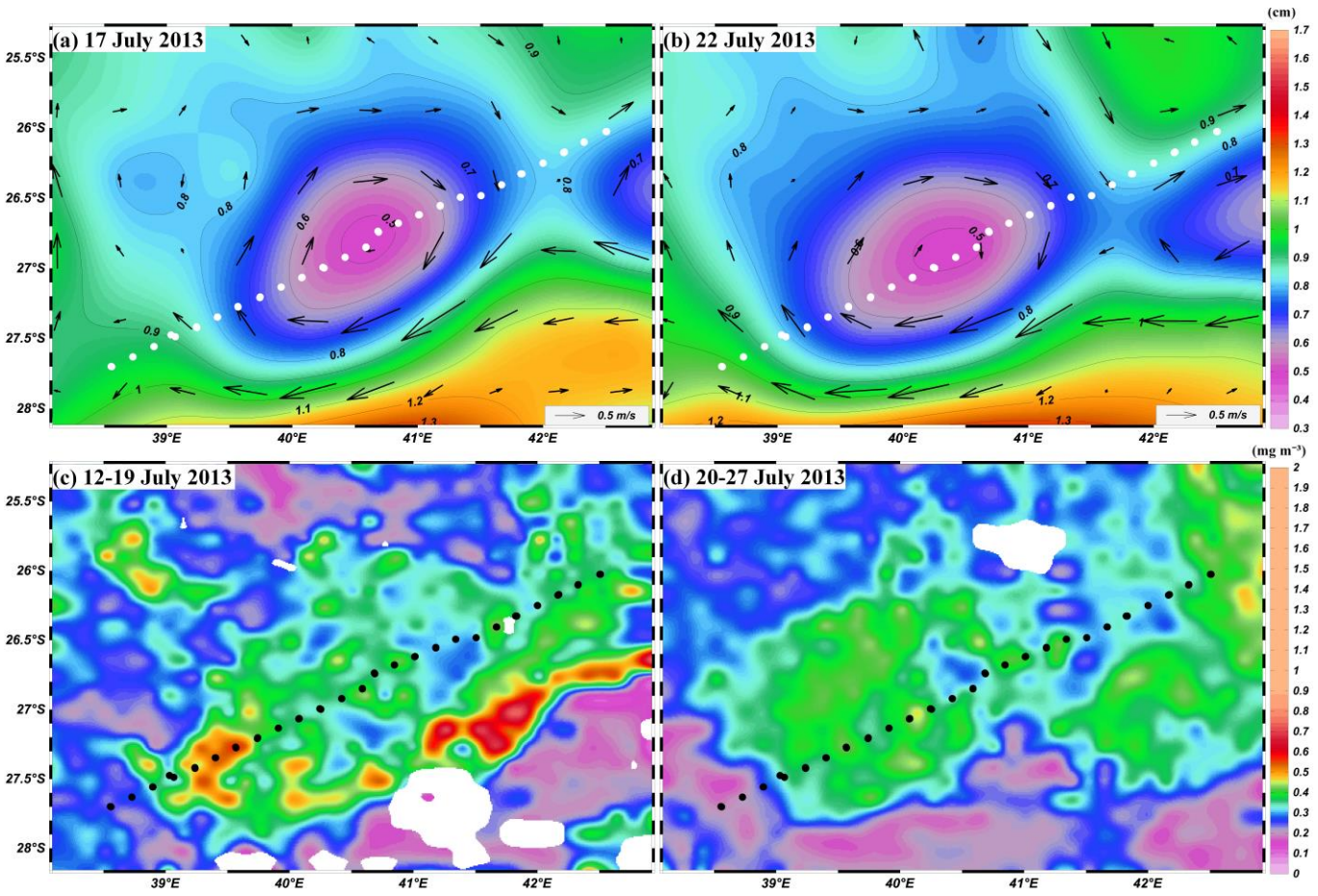
(a) 17 July 2013
(b) 22 July 2013
(c) 12-19 July 2013
(d) 20-27 July 2013
(cm)
(mg m⁻³)
0.5 m/s
25.5°S
26°S
26.5°S
27°S
27.5°S
28°S
39°E
40°E
41°E
42°E

Fig. 3

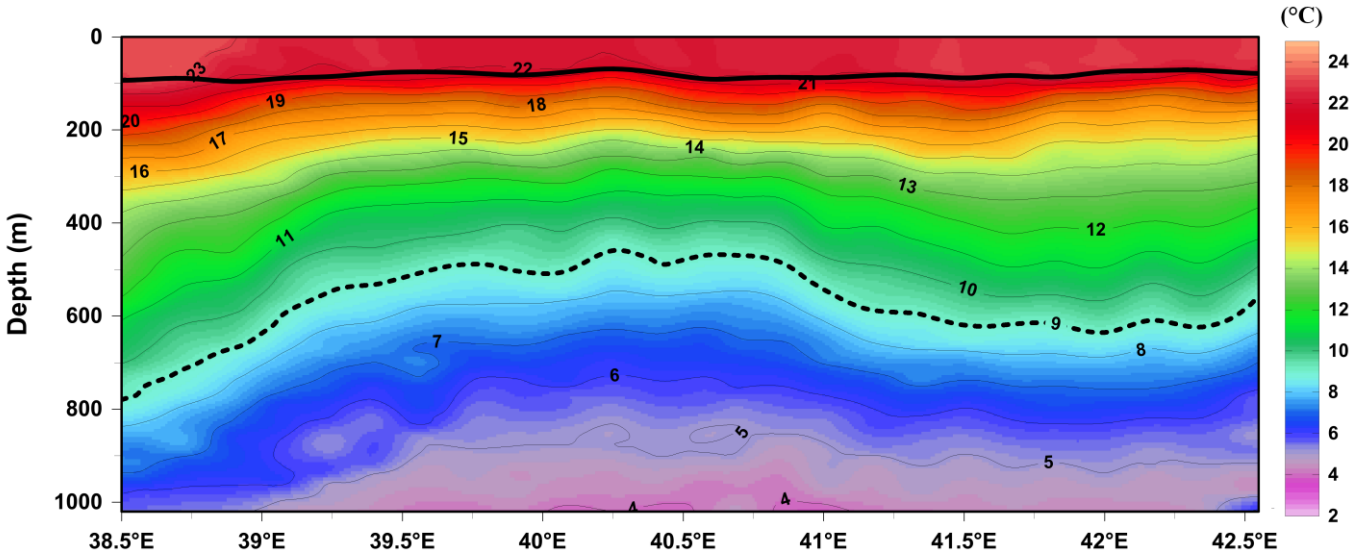
(°C)
Depth (m)
0
200
400
600
800
1000
38.5°E
39°E
39.5°E
40°E
40.5°E
41°E
41.5°E
42°E
42.5°E

691 Fig. 4
692

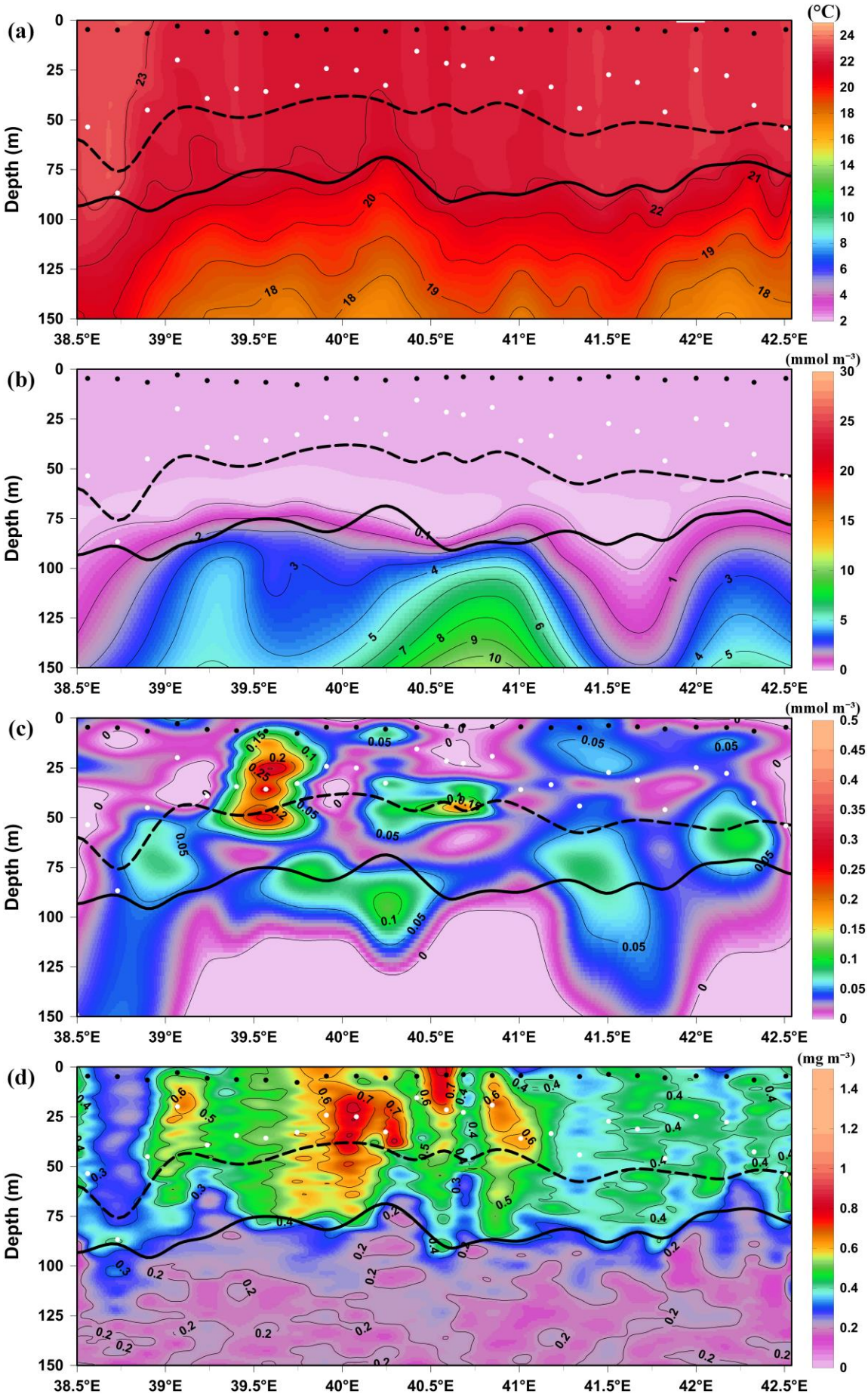

693
694

Fig. 5

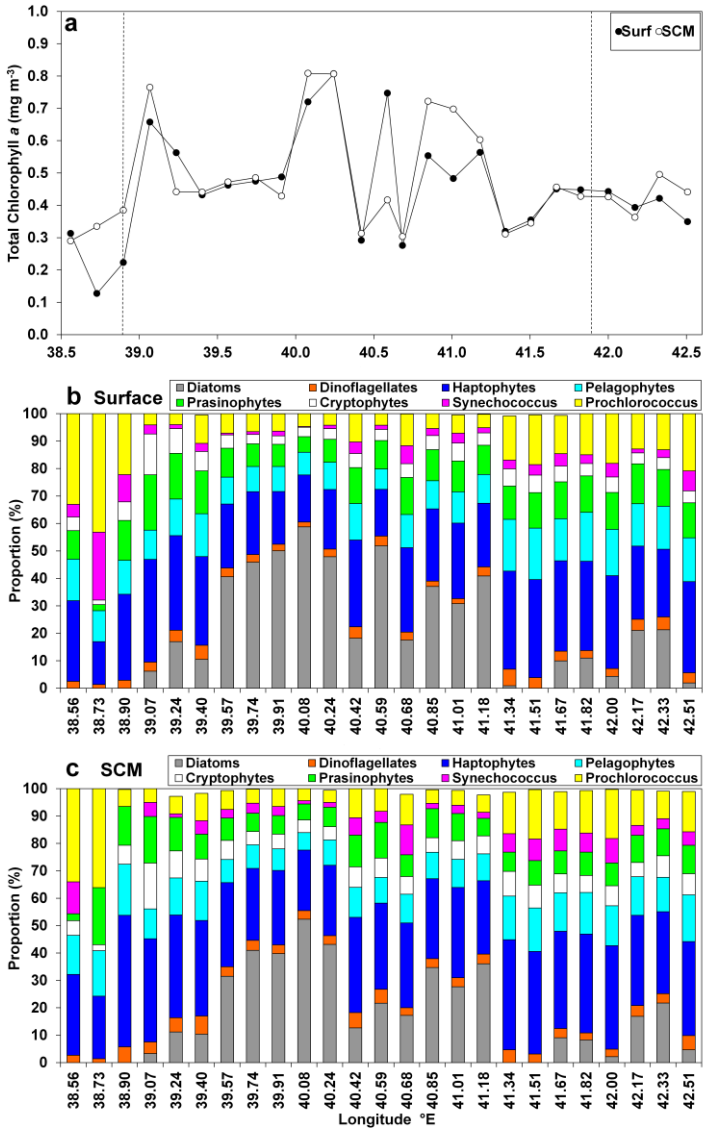
a
●Surf ○SCM
Total Chlorophyll a (mg m-3)
b Surface
c SCM
Diatoms
Dinoflagellates
Haptophytes
Pelagophytes
Prasinophytes
Cryptophytes
Synechococcus
Prochlorococcus
Proportion (%)
Longitude °E

Fig. 6

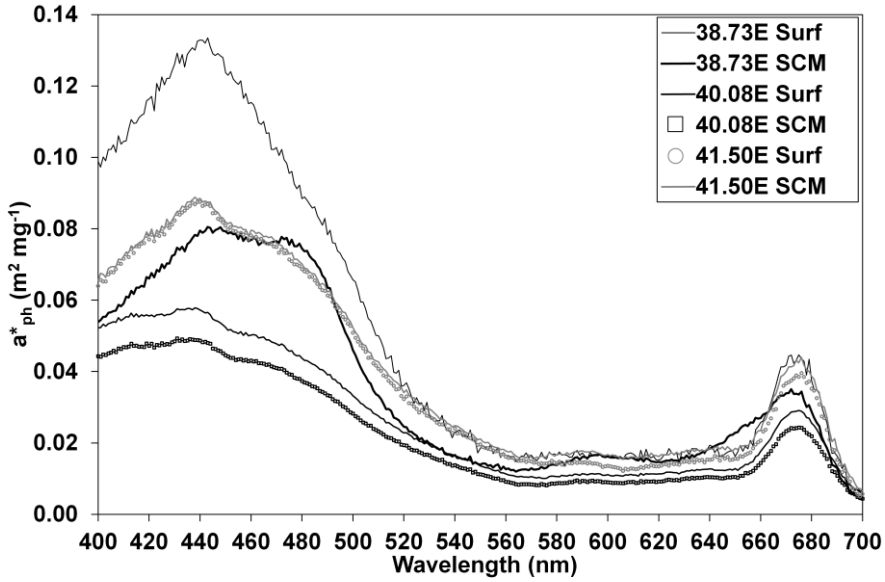
38.73E Surf
38.73E SCM
40.08E Surf
40.08E SCM
41.50E Surf
41.50E SCM
a*ph (m2 mg-1)
Wavelength (nm)

Fig. 7

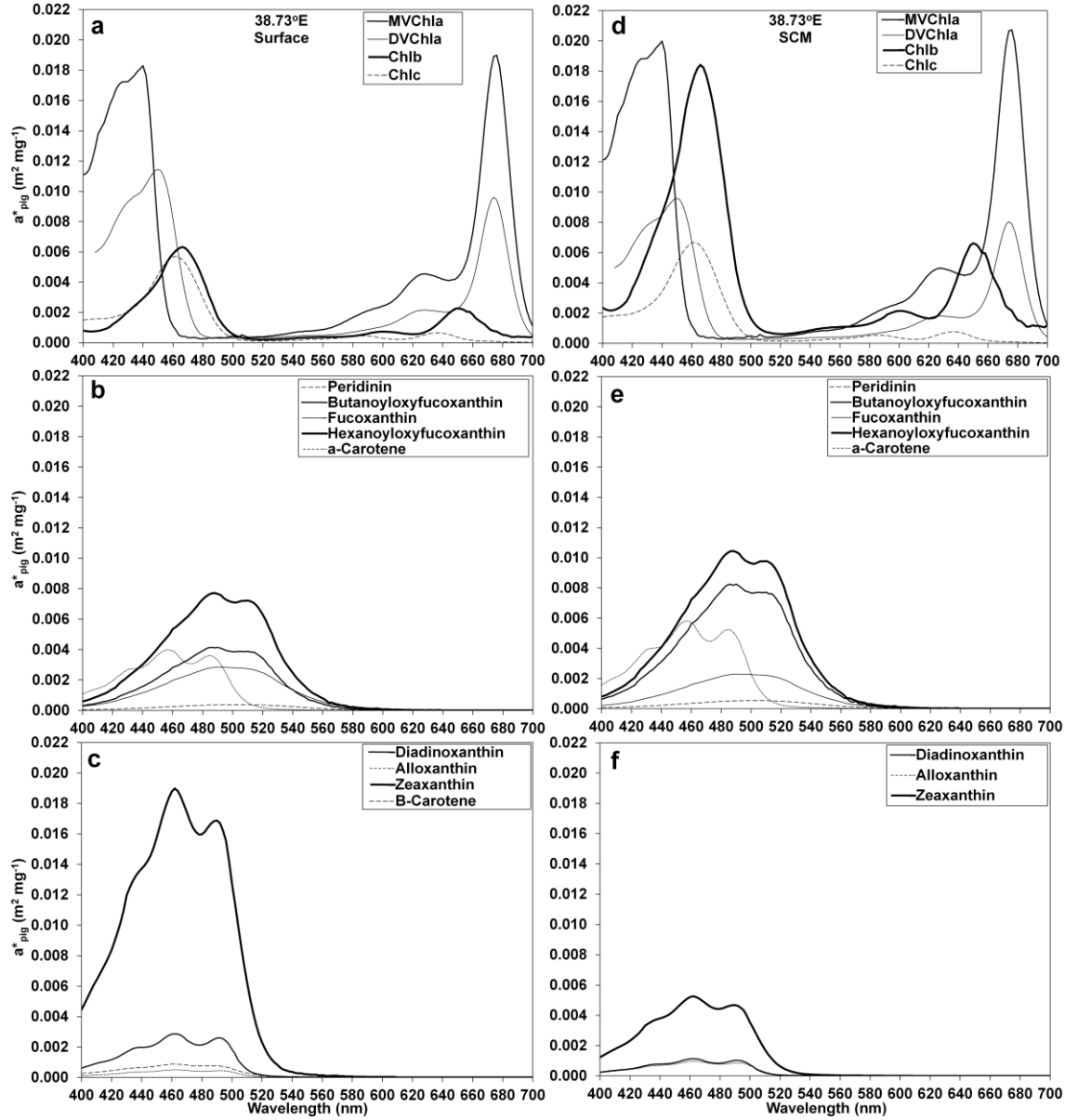
a
38.73°E
Surface
MVChla
DVChla
Chlb
Chlc
d
38.73°E
SCM
MVChla
DVChla
Chlb
Chlc
b
Peridinin
Butanoyloxyfucoxanthin
Fucoxanthin
Hexanoyloxyfucoxanthin
a-Carotene
e
Peridinin
Butanoyloxyfucoxanthin
Fucoxanthin
Hexanoyloxyfucoxanthin
a-Carotene
c
Diadinoxanthin
Alloxanthin
Zeaxanthin
B-Carotene
f
Diadinoxanthin
Alloxanthin
Zeaxanthin
a*pig (m2 mg-1)
Wavelength (nm)

Fig. 8

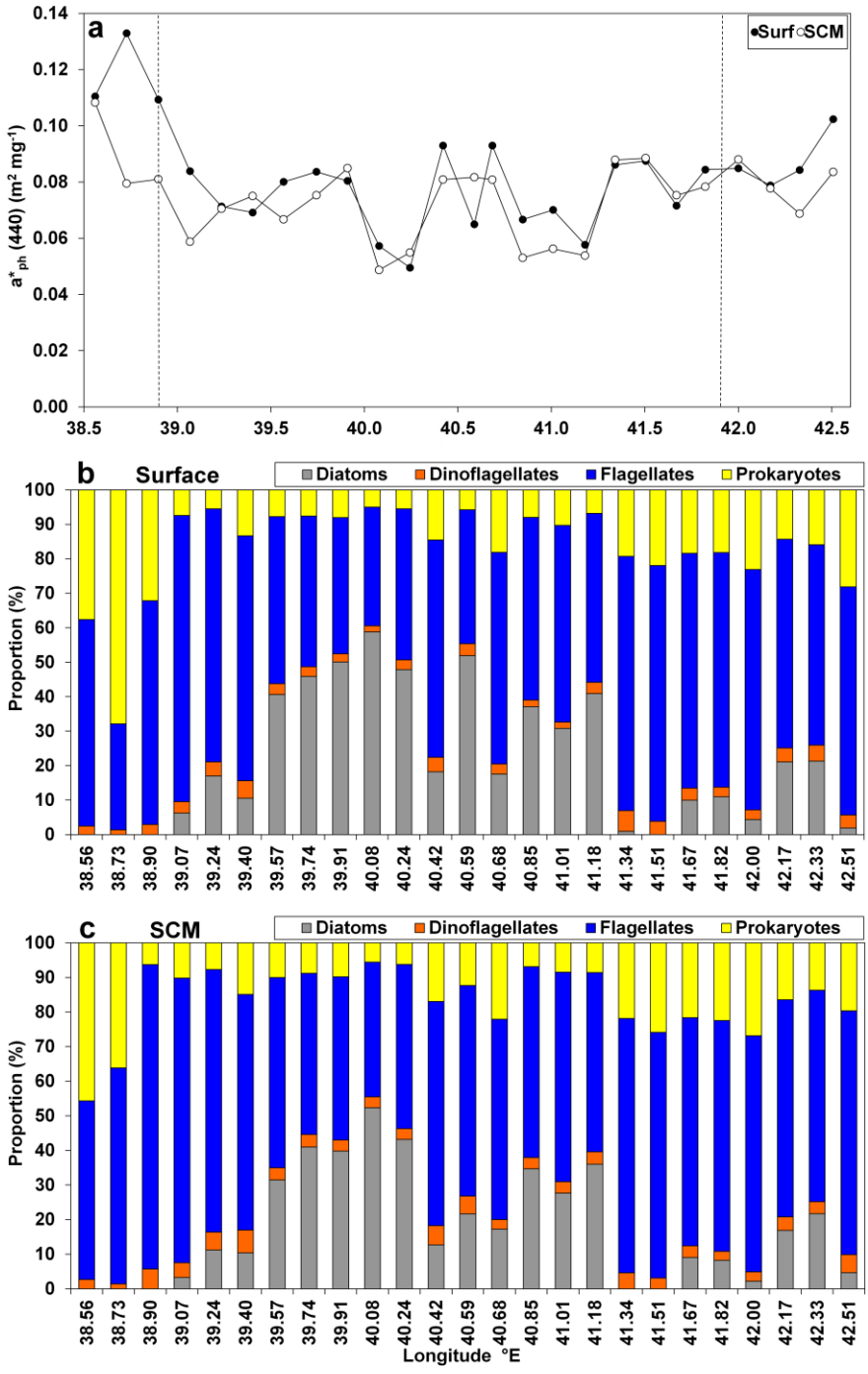
a
Surf
SCM
a^*_{ph} (440) (m^2 mg^{-1})
b
Surface
Diatoms
Dinoflagellates
Flagellates
Prokaryotes
Proportion (%)
c
SCM
Longitude °E

741 Fig. 9
742

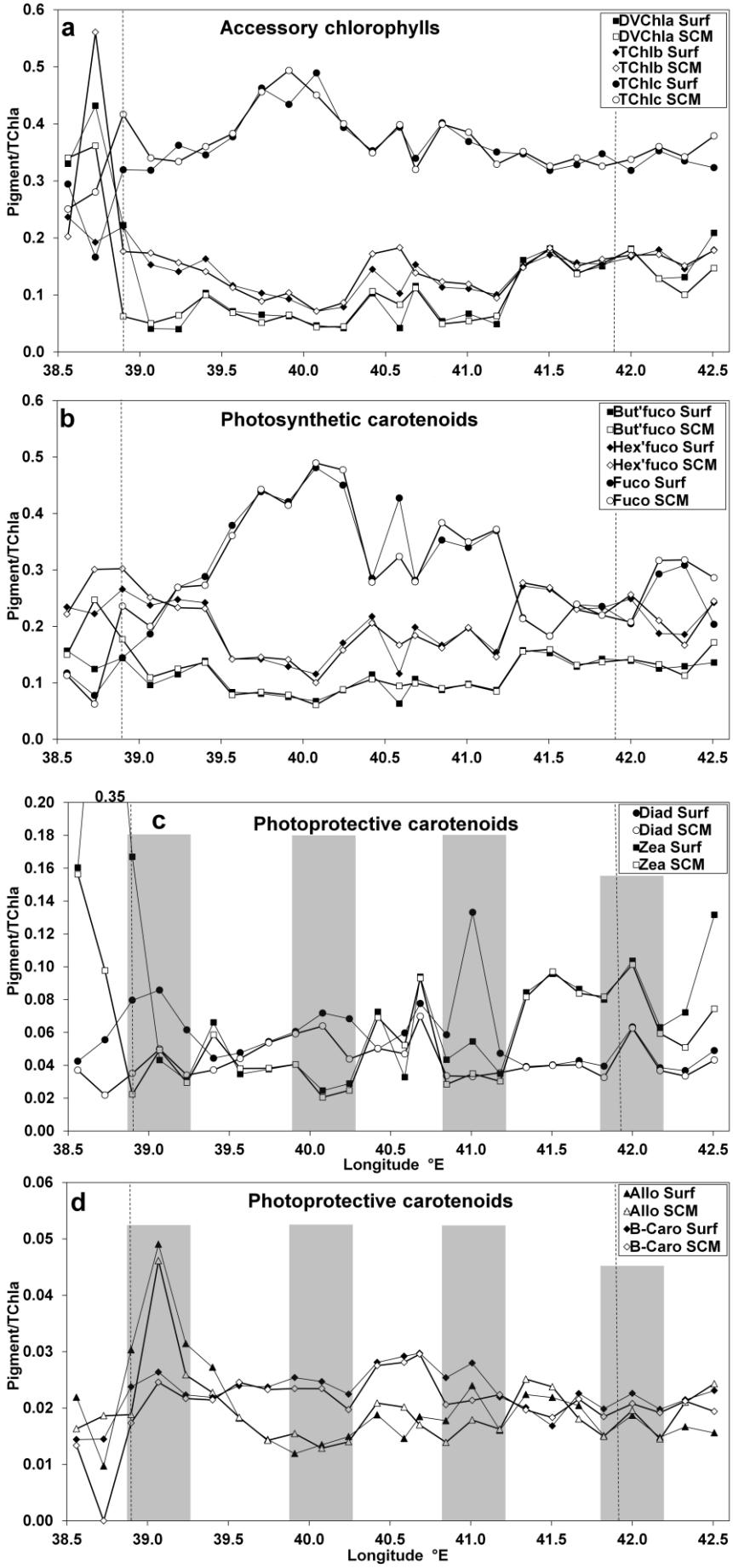

743
744

Fig. 10

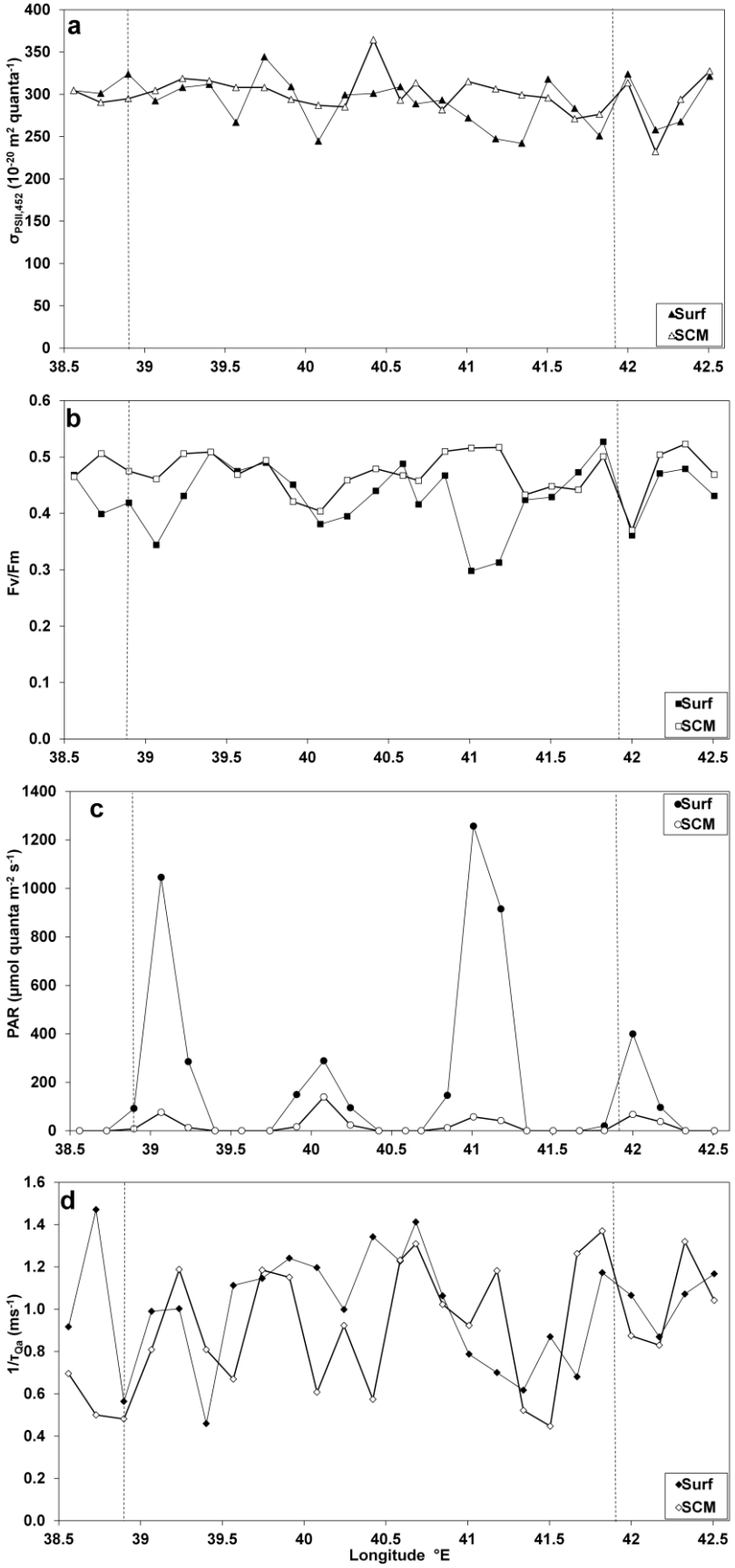
a
$\sigma_{PSII,452}$ (10^{-20} m^2 quanta^{-1})
Surf
SCM
b
Fv/Fm
Surf
SCM
c
PAR (µmol quanta m^{-2} s^{-1})
Surf
SCM
d
1/r_{Ga} (ms^{-1})
Surf
SCM
Longitude °E